Energy-Management System for a Hybrid Electric Vehicle, Using Ultracapacitors and Neural Networks

Jorge Moreno, *Member, IEEE*, Micah E. Ortúzar, *Member, IEEE*, and Juan W. Dixon, *Senior Member, IEEE*

***Abstract*—A very efficient energy-management system for hybrid electric vehicles (HEVs), using neural networks (NNs), was developed and tested. The system minimizes the energy requirement of the vehicle and can work with different primary power sources like fuel cells, microturbines, zinc-air batteries, or other power supplies with a poor ability to recover energy from a regenerative braking, or with a scarce power capacity for a fast acceleration. The experimental HEV uses lead-acid batteries, an ultracapacitor (UCAP) bank, and a brushless dc motor with nominal power of 32 kW, and a peak power of 53 kW. The digital signal processor (DSP) control system measures and stores the following parameters: primary-source voltage, car speed, instantaneous currents in both terminals (primary source and UCAP), and actual voltage of the UCAP. When UCAPs were installed on the vehicle, the increase in range was around 5.3% in city tests. However, when optimal control with NN was used, this figure increased to 8.9%. The car used for this experiment is a Chevrolet light utility vehicle (LUV) truck, similar in shape and size to Chevrolet S-10, which was converted to an electric vehicle (EV) at the Universidad Católica de Chile. Numerous experimental tests under different conditions are compared and discussed.**

***Index Terms*—Energy management, energy storage, neural networks (NNs), vehicles.**

I. Introduction

ELECTRIC vehicles have improved their performance and made suitable for commercial and domestic use during the last decades. Nevertheless, pure electric vehicles (EVs) still have not achieved ranges as good as gas-powered conventional vehicles. This problem, due to the low-energy density and specific energy contained in most electric batteries compared to that of gasoline, is resolved in hybrid vehicles by combining high-energy density of gas or hydrogen, with high efficiency of electric-drive systems [1].

Still, gas-based or hydrogen-based energy-storage systems, unlike batteries, are unable to accept energy from the regenerative braking. For this reason, these vehicles may use an auxiliary energy system (AES) able to receive regeneration and give power during peak periods. This allows using energy systems (gas turbines, fuel cells, etc.) with lower power ratings, close to the average power consumption, and at the same time, allows improving the overall vehicle efficiency [2]. Two topologies can be distinguished regarding the AES connection: parallel and series connections. Fig. 1 shows a series connection

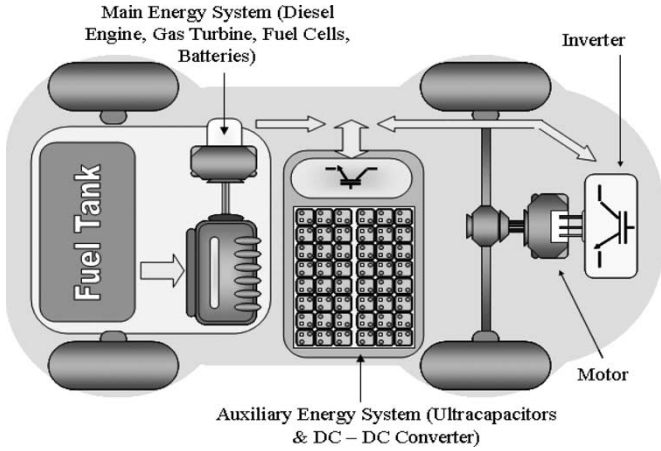

Fig. 1. Power circuit of a typical serial hybrid vehicle.

of a generic hybrid vehicle, often used in vehicles running on fuel cells, microturbines, internal combustion engines, or some kind of battery with poor specific power.

The AES shown in Fig. 1 needs to be a high-specific power device, such as ultracapacitor (UCAP), flywheel, or even a good battery pack. In this case, the UCAP looks as the most appropriate source of power because at 95% efficiency, specific power comes to 1 kW/kg [3].

For an HEV, in which batteries are in use as "main source" and UCAPs as "auxiliary source," the batteries could be used with an extended range of operation with the same state of charge (SOC) [4], [5]. However, it is essential the development of an energy-management system to control the power flow between both sources. In previous works, an approach based on SOC control of the auxiliary source was implemented [5], [6]. Nevertheless, those works did not take in account any consideration of efficiency optimization in the use of both sources.

In this paper, an optimal-control strategy, also based on SOC control of the auxiliary source was developed and tested successfully. The strategy is now based on training a neural network (NN) using the results obtained from simulations of different driving cycles. A digital signal processor (DSP) (TMS320F241) was used for real time implementation. Finally, the optimized results were compared with those obtained with the classic strategy of control proposed in a previous work [6].

The vehicle used in the driving tests is a Chevrolet "light utility vehicle (LUV)" truck (similar in weight and shape to Chevrolet S-10) with a brushless dc traction motor (nominal power of 32 and 53 kW of peak power). The main energy-storage device is formed by a pack of 26 lead-acid batteries connected in series (around 356 Vdc when fully charged) and the AES implemented with a buck–boost converter and a

Manuscript received June 3, 2004; revised November 9, 2004. Abstract published on the Internet January 25, 2006. This work was supported by Conicyt under Project Fondecyt 1020982.

The authors are with the Department of Electrical Engineering, Pontificia Universidad Católica de Chile, Santiago, Chile (e-mail: jmorenod@puc.cl; mortuzar@gmail.com; jdixon@ing.puc.cl).

Digital Object Identifier 10.1109/TIE.2006.870880

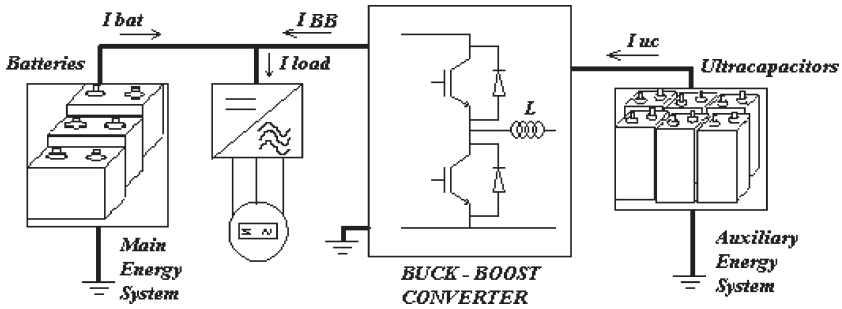

Fig. 2. Resulting power circuit in the EV.

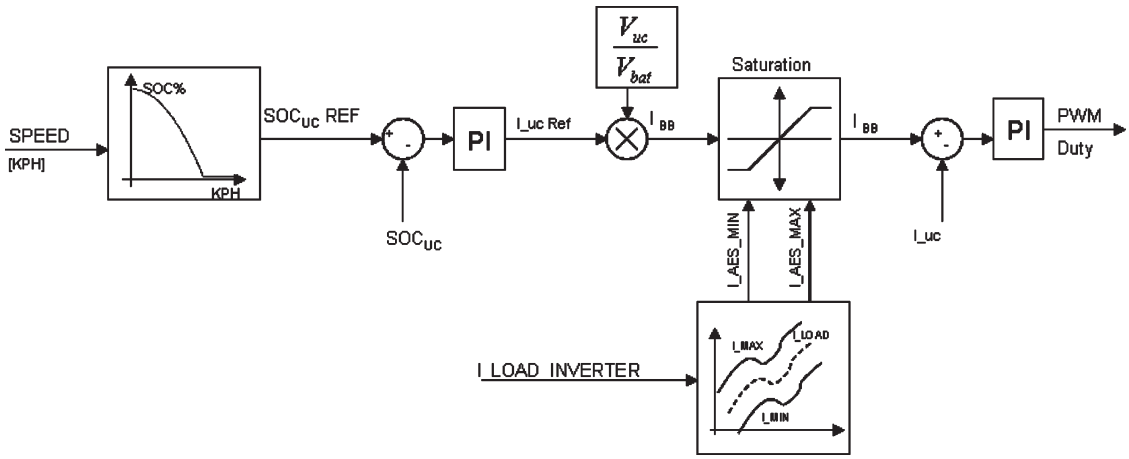

Fig. 3. Control-system diagram.

20 Farads UCAP bank, with a nominal voltage of 300 Vdc, and a nominal current of 200 Adc.

II. UCAPs Load Control

Fig. 2 shows the energy system implemented in the EV, with the main source composed by the lead-acid batteries already mentioned, and the auxiliary source implemented with the buck–boost converter and the UCAP bank. The buck–boost converter allows the energy flow from the UCAPs to the batteries or to the traction motor in both directions.

During the regenerative braking, the UCAPs store energy, and during acceleration, they provide energy to the vehicle. However, the control system must predict some driving conditions to be able to minimize the energy consumption. Some variables needed for this process are the vehicle speed, the load current, and the UCAPs charge, which is given by the capacitor voltage through

$$E_{\mathrm{uc}}^{\mathrm{rem}} = \frac{1}{2} C V_{\mathrm{uc}}^2$$

where $E_{\mathrm{uc}}^{\mathrm{rem}}$ is the remaining stored energy in the UCAP bank, C the capacitance of UCAP, and V_{uc} its terminals voltage. Considering the batteries to be a passive element, the current across them is controlled by monitoring the load current and by managing the current across the buck–boost converter. On the other hand, the UCAP charge is controlled by a second current-control loop. In addition, a special module is added to control the current limits from the batteries. The schematic is shown in Fig. 3.

The aforementioned control strategy was implemented in the DSP TMS320F241 with a monitoring system, which allows the communication in real time with a PC. Fig. 4 shows a fragment of the current of the system and the speed of the vehicle during a driving cycle. It is interesting to see that the current of the batteries has been limited to $+30$ and -3 Adc for acceleration and deceleration, respectively.

Several driving tests in a 14.2-km city loop were performed under three conditions:

1) without regeneration;
2) with regeneration but without UCAPs; and
3) with regeneration and UCAPs.

In the first case (without regeneration) the vehicle can run 2.61 km with 1 kWh of energy. In the second case, adding the regenerative-braking capability of the lead-acid batteries of the prototype, the vehicle increases its efficiency to 3.09 km/kWh, which means an efficiency increase of 18.2%. Now, when the buck–boost and UCAP system is connected, the efficiency increases to 24.4% (3.25 km/kWh). The connection of the UCAP system also reduces considerably the maximum power delivered by the main source during transient periods (lead-acid batteries in this case). It goes from more than 54 kW to only 10.7 kW.

The previous results are quite satisfactory. Nevertheless, it is possible to see that the control strategy has been designed based on the heuristic knowledge of the system and does not represent the optimal one. This work presents the design of a new strategy, in which new efficiency considerations in the operation of the system are considered.

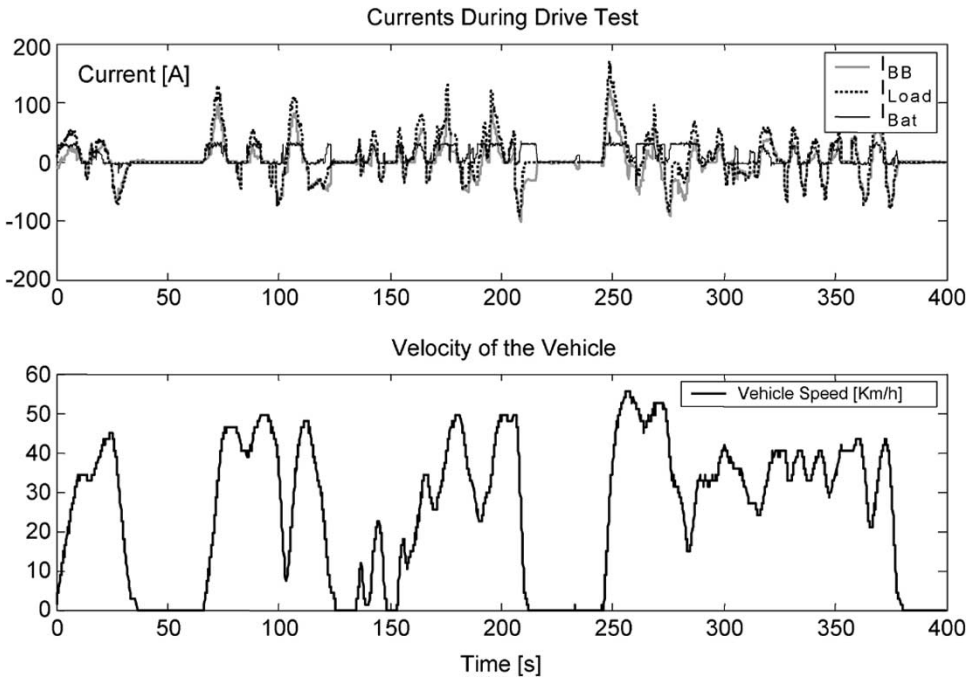

Fig. 4. Driving test fragment of currents and speed.

III. Buck–Boost Converter Model

The buck–boost converter is used for the exchange of energy between the main and the AES (Fig. 2). To improve the operation of the system, it is necessary to develop a model, able to know the efficiency as a function of the current and voltage of the UCAPs, and the battery voltage.

To simplify the model, it is assumed that the average value of the voltage in the inductance L in one period of time, is approximately zero. Making power equivalence between both sides of the converter [7], a relation for buck operation is obtained in (1), shown at the bottom of the page, where:

- D "Duty cycle" of the pulsewidth modulation (PWM) applied to the insulated gate bipolar transistor (IGBT).
- R_X Equivalent resistance of bat (battery pack), UCAPs (uc), inductance (L) or diode (inside the buck–boost converter).
- V_X Battery voltage (bat), IGBT drop or ultracapacitor voltage (uc).

It is important to mention that R_X is not a fixed number in general, but these assumptions do not affect seriously the results obtained when they are assumed constant. Particularly $R_{\rm bat}$ is very sensitive to SOC, but mainly at deep discharges. However, in the range 100%–60% (where the lead batteries being used operate), this parameter can also be considered constant. With UCAPs, Maxwell technologies, one of the most important UCAP manufacturers, defines the equivalent series resistance of a UCAP, simply by Ohm's law.

On the other hand, the duty cycle "D" can be evaluated for given values of current and voltage in (2), shown at the bottom of the page.

The efficiency relation, for a specific current and voltage of the UCAPs is obtained replacing (2) into (1). In a similar way, it is possible to obtain for a boost operation in the following expressions in (3) and (4), found at the bottom of the next page.

With these equations, the efficiency map of the converter, for each way of operation is obtained. The specific case of the boost converter is shown in Fig. 5.

IV. Optimal Control: The Model

The purpose of this paper is to find a new control strategy, for a specific driving cycle of the vehicle, able to minimize the discharge of the batteries [8]–[10]. The model should also take into account that the UCAPs are only a temporary energy source, because at the end of the driving cycle, they should remain fully charged.

$$\eta_{\rm buck} = \frac{\left[D^2 R_{\rm bat} + R_L + R_{\rm uc} + (1-D)R_d\right] V_{\rm uc}}{\left[DR_L + DR_{\rm uc} + D(1-D)R_d\right] V_{\rm bat} + D^2 R_{\rm bat}\left[DV_{\rm igbt} + V_{\rm uc} + (1-D)V_d\right]} \tag{1}$$

$$D_{1,2} = \frac{V_{\rm bat} + V_d - V_{\rm igbt} + R_d I_L \pm \sqrt{(V_d + V_{\rm bat} - V_{\rm igbt} + R_d I_L)^2 - 4R_{\rm bat} I_L \left[V_{\rm uc} + V_d + (R_L + R_{\rm uc} + R_d) I_L\right]}}{2R_{\rm bat} I_L} \tag{2}$$

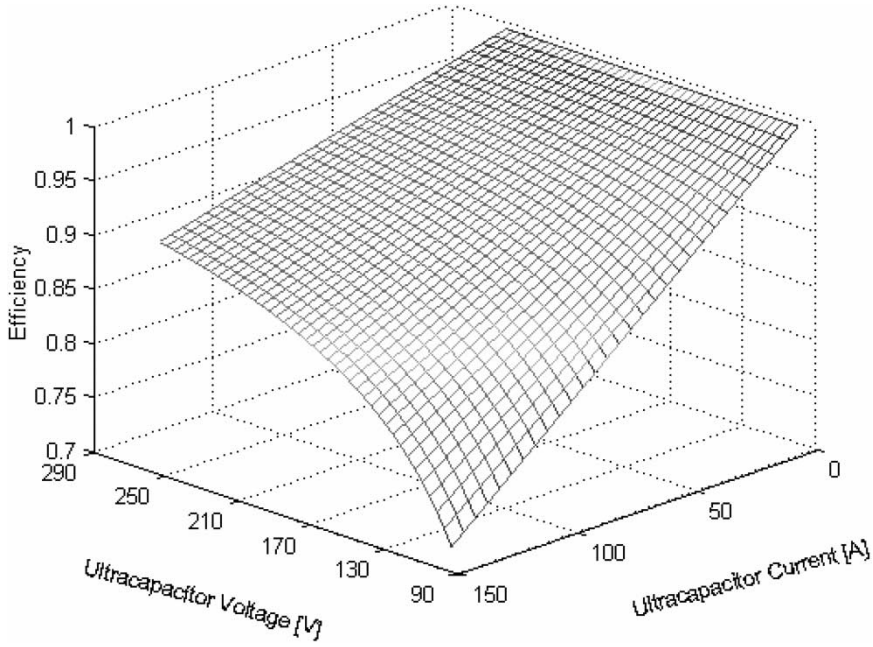

Fig. 5. Efficiency map of the boost converter.

From Fig. 2 the relation $P_{\rm load} = P_{\rm bat} + P_{\rm BB}$ is achieved, which can be written as $P_{\rm bat} = P_{\rm load} - P_{\rm BB}$. Considering that SOC of batteries and UCAPs can be associated with their respective remaining energy $E_{\rm bat}^{\rm rem}$ and $E_{\rm uc}^{\rm rem}$, and on the other hand, these energies are state variables of the system, the equations that deal with the dynamics of the system are

$$\begin{aligned} E_{\rm bat}^{\rm rem}(k+1) &= E_{\rm bat}^{\rm rem}(k) + [P_{\rm BB}(k) - P_{\rm load}(k)] \cdot \eta_{\rm bat} \cdot \Delta T \\ E_{\rm uc}^{\rm rem}(k+1) &= E_{\rm uc}^{\rm rem}(k) - P_{\rm uc} \cdot \Delta T \end{aligned} \tag{5}$$

where ΔT is the sampling time between k and $k+1$ and $\eta_{\rm bat}$ is the efficiency of the batteries energy conversion.

The variable that has to be minimized is the battery discharge, which can be expressed as

$$J = \sum_{k=0}^{N-1} \dot{E}_{\rm bat}^{\rm rem}\left[I_{\rm bat}(k)\right] \cdot \Delta T.$$

On the other hand, the buck–boost power at the battery side, given as a function of UCAP voltage and current is

$$\begin{aligned} P_{\rm BB}(k) &= I_{\rm BB}(k) \cdot V_{\rm bat}(k) \\ &= I_{\rm uc}(k) \cdot V_{\rm uc}(k) \cdot \eta_{\rm BB}\left[V_{\rm uc}(k), I_{\rm uc}(k)\right] \end{aligned}$$

where $\eta_{\rm BB}[V_{\rm uc}(k), I_{\rm uc}(k)]$ is the buck–boost converter efficiency.

It is necessary to incorporate into the model the restriction $E_{\rm uc}^{\rm rem}(N) = E_{\rm uc}^{\rm rem}(0)$, which ensures that the UCAPs charge will remain the same at the end of the driving cycle. Then, the optimal-control-model approach becomes

$$\text{Min} \quad J = \phi\left[E_{\rm uc}^{\rm rem}(N)\right] + \sum_{k=0}^{N-1} \dot{E}_{\rm bat}^{\rm rem}\left[I_{\rm load}(k), I_{\rm BB}(k)\right] \cdot \Delta T$$

Subject to

$$\begin{aligned} E_{\rm bat}^{\rm rem}(k+1) &= E_{\rm bat}^{\rm rem}(k) - P_{\rm load}(k) \cdot \eta_{\rm bat} \cdot \Delta T + I_{\rm uc}(k) \\ &\quad \times V_{\rm uc}\left\lfloor E_{\rm uc}^{\rm rem}(k), I_{\rm uc}(k)\right\rfloor \\ &\quad \times \eta_{\rm BB}\left[V_{\rm uc}(k), I_{\rm uc}(k)\right] \cdot \eta_{\rm bat} \cdot \Delta T \\ E_{\rm uc}^{\rm rem}(k+1) &= E_{\rm uc}^{\rm rem}(k) - \eta_{\rm uc} \cdot I_{\rm uc}(k) \\ &\quad \times V_{\rm uc}\left[E_{\rm uc}^{\rm rem}(k), I_{\rm uc}(k)\right] \cdot \Delta T. \end{aligned} \tag{6}$$

Defining the state variable

$$x(k) = \left[E_{\rm bat}^{\rm rem}(k) \quad E_{\rm uc}^{\rm rem}(k)\right]^T.$$

For simplification, the motor-inverter system of the vehicle will be considered a "black box" whose power requirements are known for a given driving cycle, and then it is not possible to influence the current $I_{\rm load}$. As it was previously mentioned, the EV has a data-acquisition system that allows knowing the

$$\eta_{\rm boost} = \frac{R_{\rm bat}(1-D)^2\left[1-(1-D)\frac{V_d}{V_{\rm uc}} - D\frac{V_{\rm igbt}}{V_{\rm uc}}\right] + (1-D)\left[R_{\rm uc}+R_L+(1-D)R_d\right]\frac{V_{\rm bat}}{V_{\rm uc}}}{R_{\rm uc}+R_L+(1-D)R_d+(1-D)^2R_{\rm bat}} \tag{3}$$

$$D_{1,2} = \frac{V_d + V_{\rm bat} - V_{\rm igbt} + (R_d+2R_{\rm bat})I_L \pm \sqrt{\begin{array}{l}\left[(R_d+2R_{\rm bat})I_L + V_d + V_{\rm bat} - V_{\rm igbt}\right]^2 \\ -4R_{\rm bat}I_L\left[(R_{\rm bat}+R_d+R_L+R_{\rm uc})I_L - V_{\rm uc} + V_d + V_{\rm bat}\right]\end{array}}}{2R_{\rm bat}I_L} \tag{4}$$

load current in the driving cycle. Then, the variable $\dot{E}_{\rm bat}^{\rm rem}$ will depend only on the UCAPs current, which means $\dot{E}_{\rm bat}^{\rm rem}[I_{\rm uc}(k)]$.

V. Numerical Resolution for Optimal Condition

It has to be found a control sequence I_{uc}^{*}, $0 \le k \le N$ and the trajectory $x(k)$, to find the solution at the set of equations

$$\dot{x}(k+1) = f^k\left[x(k), I_{\rm uc}(k)\right] \qquad x(0) \text{ given.} \tag{7}$$

Minimizing the following cost function

$$J = \phi\left[E_{\rm uc}^{\rm rem}(N)\right] + \sum_{k=0}^{N-1} \dot{E}_{\rm bat}^{\rm rem}\left[I_{\rm uc}(k)\right] \cdot \Delta T. \tag{8}$$

Defining the Lagrangian equation as

$$L^k\left[x(k), I_{\rm uc}(k)\right] = \dot{E}_{\rm bat}^{\rm rem}\left[I_{\rm uc}(k)\right] \cdot \Delta T$$

and the Hamiltonian

$$H^k = L^k\left[x(k), I_{\rm uc}(k)\right] + \lambda^T(k+1) f^k\left[x(k), I_{\rm uc}(k)\right] \qquad i = 0, 1, \ldots, N-1.$$

The solution must satisfy Euler–Lagrange equations

$$\lambda(k) = \left[\frac{\partial f^k}{\partial x(k)}\right]^T \lambda(k+1) + \left[\frac{\partial L^k}{\partial x(k)}\right]^T. \tag{9}$$

Subject to the final condition

$$\lambda(N) = \left[\frac{\partial \phi}{\partial x(N)}\right]^T. \tag{10}$$

Finally, the optimality condition is given by the following relation

$$\frac{\partial H^k}{\partial I_{\rm uc}(k)} = \frac{\partial L^k}{\partial I_{\rm uc}(k)} + \lambda^T(k+1)\frac{\partial f^k}{\partial I_{\rm uc}(k)} = 0. \tag{11}$$

Applying the optimality conditions to the model given by (6), it yields

$$\begin{aligned} L^k\left[x(k), I_{\rm uc}(k)\right] &= \dot{E}_{\rm bat}^{\rm rem}(k) \cdot \Delta T \\ &= E_{\rm bat}^{\rm rem}(k+1) - E_{\rm bat}^{\rm rem}(k) \\ &= I_{\rm uc}(k) \cdot V_{\rm uc}\left[E_{\rm uc}^{\rm rem}(k), I_{\rm uc}(k)\right] \\ &\quad \times \eta_{\rm BB}\left[V_{\rm uc}(k), I_{\rm uc}(k)\right] \cdot \eta_{\rm bat} \cdot \Delta T \\ &\quad - P_{\rm load}(k) \cdot \eta_{\rm bat} \cdot \Delta T \end{aligned} \tag{12}$$

and then

$$\begin{aligned} \frac{\partial L^k}{\partial I_{\rm uc}(k)} &= \frac{\partial \dot{E}_{\rm bat}^{\rm rem}(k) \cdot \Delta T}{\partial I_{\rm uc}} \\ &= V_{\rm uc}\left[E_{\rm uc}^{\rm rem}(k), I_{\rm uc}(k)\right] \cdot \eta_{\rm BB}\left[V_{\rm uc}(k), I_{\rm uc}(k)\right] \\ &\quad \times \eta_{\rm bat} \cdot \Delta T + I_{\rm uc}(k) \cdot \frac{\partial V_{\rm uc}\left[E_{\rm uc}^{\rm rem}(k), I_{\rm uc}(k)\right]}{\partial I_{\rm uc}} \\ &\quad \times \eta_{\rm BB}\left[V_{\rm uc}(k), I_{\rm uc}(k)\right] \cdot \eta_{\rm bat} \cdot \Delta T + I_{\rm uc}(k) \\ &\quad \times V_{\rm uc}\left[E_{\rm uc}^{\rm rem}(k), I_{\rm uc}(k)\right] \cdot \frac{\partial \eta_{\rm BB}\left[V_{\rm uc}(k), I_{\rm uc}(k)\right]}{\partial I_{\rm uc}} \\ &\quad \times \eta_{\rm bat} \cdot \Delta T. \end{aligned} \tag{13}$$

Now, the derivatives in (9) are defined as

$$\frac{\partial f^k}{\partial x(k)} = \begin{bmatrix} \frac{\partial f^1}{\partial E_{\rm bat}^{\rm rem}} & \frac{\partial f^2}{\partial E_{\rm bat}^{\rm rem}} \\ \frac{\partial f^1}{\partial E_{\rm uc}^{\rm rem}} & \frac{\partial f^2}{\partial E_{\rm uc}^{\rm rem}} \end{bmatrix} \quad \frac{\partial L^k}{\partial x(k)} = \begin{bmatrix} \frac{\partial L}{\partial E_{\rm bat}^{\rm rem}} \\ \frac{\partial L}{\partial E_{\rm uc}^{\rm rem}} \end{bmatrix}. \tag{14}$$

Evaluating each one of the terms given by (14)

$$\frac{\partial f^1}{\partial E_{\rm bat}^{\rm rem}} = 1 \quad \frac{\partial f^2}{\partial E_{\rm bat}^{\rm rem}} = 0 \quad \frac{\partial L}{\partial E_{\rm bat}^{\rm rem}} = 0 \tag{15}$$

$$\begin{aligned} \frac{\partial f^1}{\partial E_{\rm uc}^{\rm rem}} &= \frac{\partial I_{\rm uc}(k)}{\partial E_{\rm uc}^{\rm rem}} \cdot V_{\rm uc}\left[E_{\rm uc}^{\rm rem}(k), I_{\rm uc}(k)\right] \\ &\quad \times \eta_{\rm BB}\left[V_{\rm uc}(k), I_{\rm uc}(k)\right] \cdot \eta_{\rm bat} \cdot \Delta T + I_{\rm uc}(k) \\ &\quad \times \frac{\partial V_{\rm uc}\left[E_{\rm uc}^{\rm rem}(k), I_{\rm uc}(k)\right]}{\partial E_{\rm uc}^{\rm rem}} \cdot \eta_{\rm BB}\left[V_{\rm uc}(k), I_{\rm uc}(k)\right] \\ &\quad \times \eta_{\rm bat} \cdot \Delta T + I_{\rm uc}(k) \cdot V_{\rm uc}\left[E_{\rm uc}^{\rm rem}(k), I_{\rm uc}(k)\right] \\ &\quad \times \frac{\partial \eta_{\rm BB}\left[V_{\rm uc}(k), I_{\rm uc}(k)\right]}{\partial E_{\rm uc}^{\rm rem}} \cdot \eta_{\rm bat} \cdot \Delta T \end{aligned} \tag{16}$$

$$\begin{aligned} \frac{\partial f^2}{\partial E_{\rm uc}^{\rm rem}} &= 1 - \frac{\partial I_{\rm uc}(k)}{\partial E_{\rm uc}^{\rm rem}} \cdot V_{\rm uc}\left[E_{\rm uc}^{\rm rem}(k), I_{\rm uc}(k)\right] \cdot \eta_{\rm uc} \cdot \Delta T \\ &\quad - I_{\rm uc}(k) \cdot \frac{\partial V_{\rm uc}\left[E_{\rm uc}^{\rm rem}(k), I_{\rm uc}(k)\right]}{\partial E_{\rm uc}^{\rm rem}} \cdot \eta_{\rm uc} \cdot \Delta T \end{aligned} \tag{17}$$

$$\begin{aligned} \frac{\partial L}{\partial E_{\rm uc}^{\rm rem}} &= \frac{\partial I_{\rm uc}(k)}{\partial E_{\rm uc}^{\rm rem}} \cdot V_{\rm uc}\left[E_{\rm uc}^{\rm rem}(k), I_{\rm uc}(k)\right] \\ &\quad \times \eta_{\rm BB}\left[V_{\rm uc}(k), I_{\rm uc}(k)\right] \cdot \eta_{\rm bat} \cdot \Delta T + I_{\rm uc}(k) \\ &\quad \times \frac{\partial V_{\rm uc}\left[E_{\rm uc}^{\rm rem}(k), I_{\rm uc}(k)\right]}{\partial E_{\rm uc}^{\rm rem}} \cdot \eta_{\rm BB}\left[V_{\rm uc}(k), I_{\rm uc}(k)\right] \\ &\quad \times \eta_{\rm bat} \cdot \Delta T + I_{\rm uc}(k) \cdot V_{\rm uc}\left[E_{\rm uc}^{\rm rem}(k), I_{\rm uc}(k)\right] \\ &\quad \times \frac{\partial \eta_{\rm BB}\left[V_{\rm uc}(k), I_{\rm uc}(k)\right]}{\partial E_{\rm uc}^{\rm rem}} \cdot \eta_{\rm bat} \cdot \Delta T. \end{aligned} \tag{18}$$

Replacing (15)–(18) into (9), the optimality condition for λ_1 and λ_2 is obtained

$$\begin{aligned} \lambda_1(k+1) &= \lambda_1(k) \\ \lambda_2(k) &= \lambda_1(k+1) \cdot \text{ec16} + \lambda_2(k+1) \cdot \text{ec17} + \text{ec18} \end{aligned} \tag{19}$$

where the terms ec16, ec17, and ec18 are the corresponding expressions of (16)–(18), respectively.

Equation (10) has given the final condition for lambda and hence

$$\lambda_2(N) = \left[\frac{\partial \phi}{\partial E_{\rm uc}^{\rm rem}(N)}\right]^T = 2\left[E_{\rm uc}^{\rm rem}(N) - E_{\rm uc}^{\rm rem}(0)\right]. \tag{20}$$

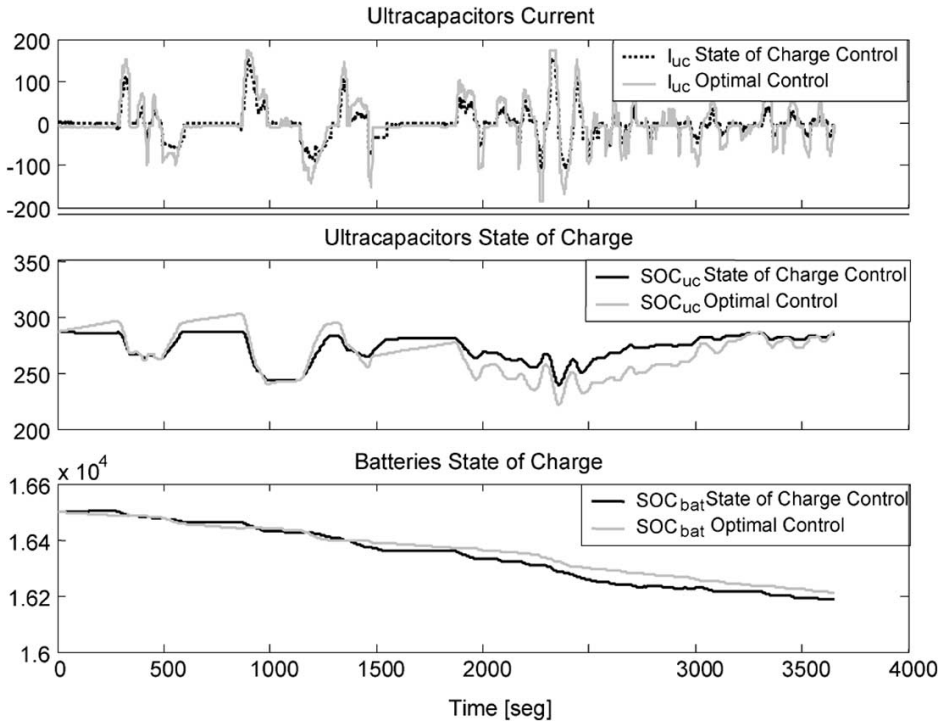

Fig. 6. Optimal-control applied to buck–boost system.

The third condition of optimality is given by (11), where

$$\frac{\partial f^1}{\partial I_{\rm uc}} = V_{\rm uc}\left[E_{\rm uc}^{\rm rem}(k), I_{\rm uc}(k)\right] \cdot \eta_{\rm BB}\left[V_{\rm uc}(k), I_{\rm uc}(k)\right] \cdot \eta_{\rm bat} \times \Delta T + I_{\rm uc}(k) \cdot \frac{\partial V_{\rm uc}\left[E_{\rm uc}^{\rm rem}(k), I_{\rm uc}(k)\right]}{\partial I_{\rm uc}} \times \eta_{\rm BB}\left[V_{\rm uc}(k), I_{\rm uc}(k)\right] \cdot \eta_{\rm bat} \cdot \Delta T + I_{\rm uc}(k) \times V_{\rm uc}\left[E_{\rm uc}^{\rm rem}(k), I_{\rm uc}(k)\right] \cdot \frac{\partial \eta_{\rm BB}\left[V_{\rm uc}(k), I_{\rm uc}(k)\right]}{\partial I_{\rm uc}} \times \eta_{\rm bat} \cdot \Delta T \quad (21)$$

$$\frac{\partial f^2}{\partial I_{\rm uc}} = -V_{\rm uc}\left[E_{\rm uc}^{\rm rem}(k), I_{\rm uc}(k)\right] \cdot \eta_{\rm uc} \cdot \Delta T - I_{\rm uc}(k) \times \frac{\partial V_{\rm uc}\left[E_{\rm uc}^{\rm rem}(k), I_{\rm uc}(k)\right]}{\partial I_{\rm uc}} \cdot \eta_{\rm uc} \cdot \Delta T \quad (22)$$

and finally

$$\frac{\partial L}{\partial I_{\rm uc}} + \lambda_1(k+1) \cdot \text{ec21} + \lambda_1(k+1) \cdot \text{ec22} = 0 \quad (23)$$

where ec 21 and ec 22 are nominations for (21) and (22), respectively. Besides, $\partial L/\partial I_{\rm uc}$ is given by (13).

In the above equations, the expressions: $(\partial \eta_{\rm BB}[V_{\rm uc}(k), I_{\rm uc}(k)])/\partial E_{\rm uc}^{\rm rem}$ and $(\partial \eta_{\rm BB}[V_{\rm uc}(k), I_{\rm uc}(k)])/\partial I_{\rm uc}$ were obtained numerically from (1)–(4).

To solve the system given by the set of equations (6), (19), (20), and (23) the gradient method will be applied. The particularity of this method is that the equations that govern the dynamics of the system are solved exactly in each iteration, by perturbing the control variable every time, to approach the ideal solution. In other words, the algorithm simulates the dynamic response of the system changing the history of the control variable in each iteration. In this way, the physical effect that takes place in the optimization is visible in each step [11].

The method begins with the initial conditions specification, and a nominal path for the control ($I_{\rm uc}$). It is necessary to integrate (6) from t_0 to t_f to get $x_0(t)$, vector that represents the initial path for the state variables. At the same time, the cost function, and the sensitivity matrix $F(t)$, $(\partial f/\partial x)$, and G(t),$(\partial f/\partial I_{\rm uc})$, which correspond to the Lagrangian Gradients [$L_x(t)$ and $L_{I_{\rm uc}}(t)$], respectively, are evaluated. Then, the associated vector is integrated backward from the final condition to obtain $\lambda_0(t)$. Once $\lambda_0(t)$ is obtained, it is possible to determine $H_{I_{\rm uc}}(t)$. In the first iterations, $H_{I_{\rm uc}}(t)$ will not be close to zero because the initial chosen path for the control is not optimal. Then, in the following iteration, the history of the control is disturbed by a function of $H_{I_{\rm uc}}(\rm t)$ and the process is repeated until the solution is close enough to the optimal value.

One perturbation option for the variable of control is

$$I_{\rm uc}^{i+1}(k) = I_{\rm uc}^{i}(k) - \varepsilon_i \left[\frac{\partial H(k)}{\partial I_{\rm uc}}\right]_i^T$$

where ε_i is a scalar. This method is also known as "steepest descendent" algorithm.

VI. Simulations

A simulation program has been implemented in Matlab for the aforementioned system. To simulate the electrical vehicle behavior, different drive cycles around the city have been performed, from where the motor-drive currents, as a function of time, were obtained. This is possible because the EV and the data-acquisition system were already implemented.

Then, for each one of the drive cycles, the system was simulated according to (6), taking as information the input

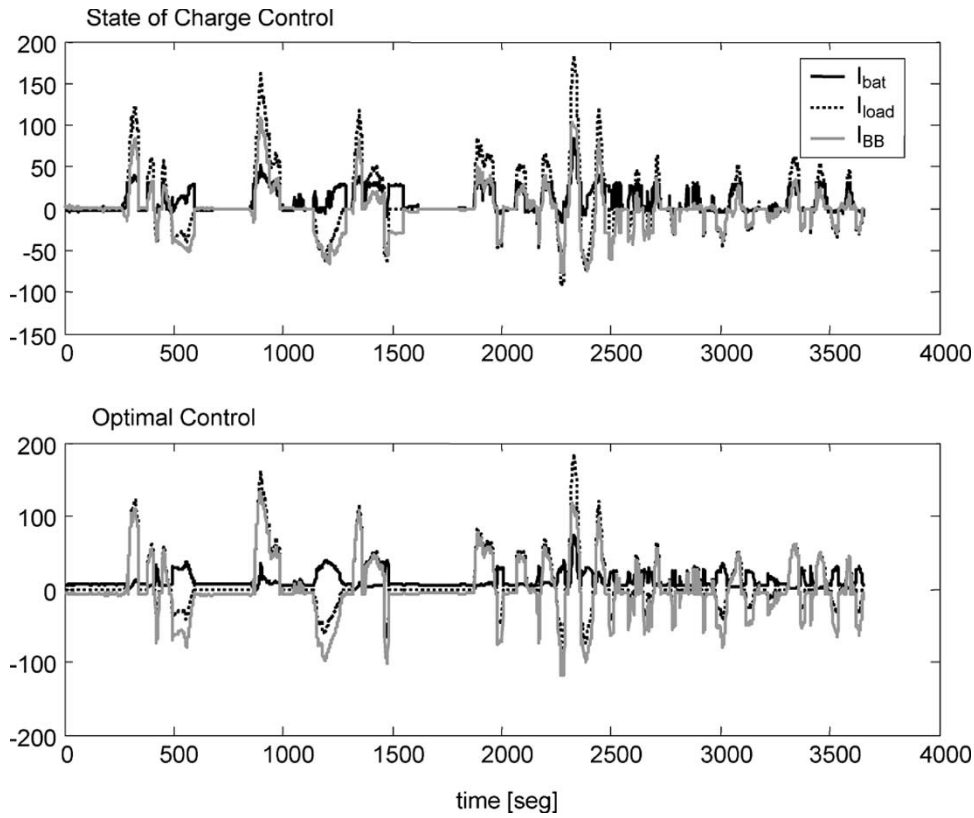

Fig. 7. Comparison of the two control strategies (load, battery, and buck–boost current).

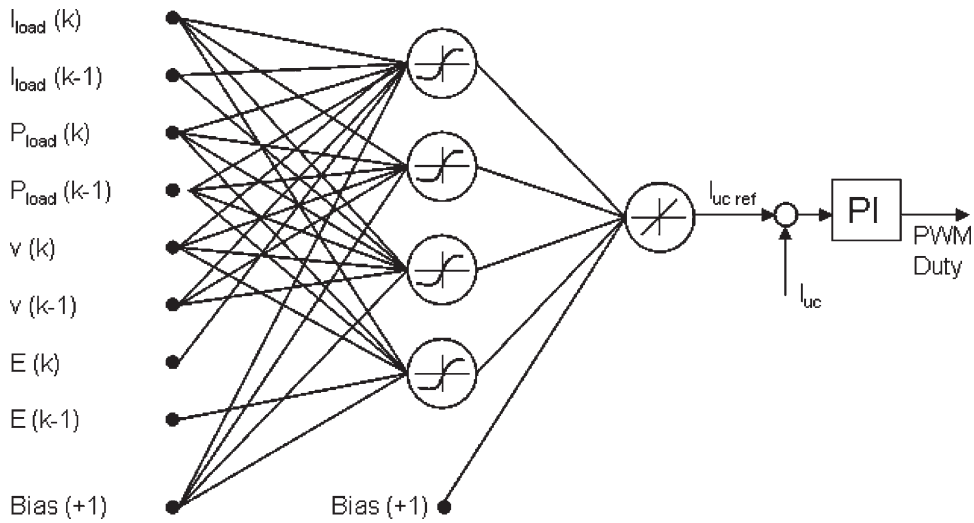

Fig. 8. Trained NNs.

currents of the load in each instant. On the other hand, the initial conditions of batteries and UCAPs are also known.

The final objective is to determine the optimal current that the buck–boost converter must deliver. To begin the iteration with the gradient method, it is necessary to establish a history of the nominal control. In this case, the control variable is $I_{\rm uc}$, which, for the first iteration, is assumed to be a linear function of the load current. Once these parameters have been established, the system is solved through (7)–(11), and then the results of Fig. 6 are obtained. The figure shows a comparison between normal control and optimized control.

It is observed that the optimal control fulfils one of the restrictions proposed in the algorithm, that is, the final charge condition of the UCAPs remains the same as their initial conditions. On the other hand, the reference current for the buck–boost converter has notably reduced the deep of discharge of the batteries and, after 30 different driving cycles, an average improvement of around 5% was obtained.

Fig. 7 shows the results obtained at the high-voltage side of the buck–boost converter. It is possible to see that, using this new strategy, the current's variability of the battery is smaller.

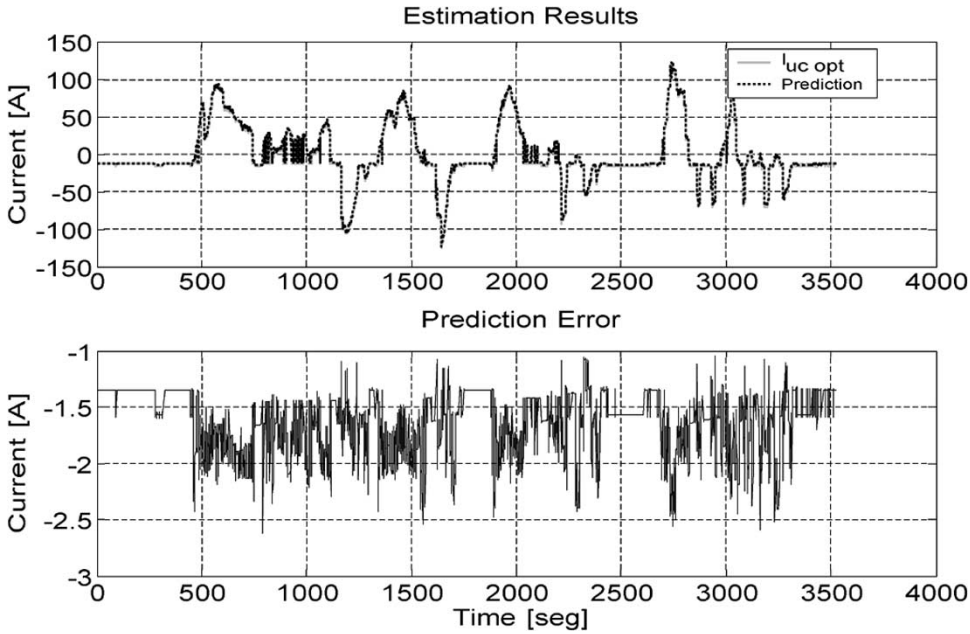

Fig. 9. Simulation results for a specific data set.

TABLE I
ROAD TESTS RESULTS

	Drive City Circuit (Km)	Kwh Used	Ah Used	Km/KWh	Km/KWh Improvement
Batteries without Regeneration	14.2	5.45	13.90	2.61	-
Batteries with Regeneration	14.2	4.6125	11.23	3.09	18.2%
Batteries with AES (SOC Control)	14.2	4.36	10.55	3.25	24.4%
Batteries with AES (Optimal Neural Network Control)	14.2	4.24	10.58	3.36	28.7%

VII. PRACTICAL APPROACH: EXTENSION TO NNS

In recent years, the development of the artificial intelligence (AI) has been remarkable. Its importance lies in the capacity to represent or emulate human knowledge to memorize, acquire knowledge, perceive, and take intelligent decisions. Within this field, we can find the application of NNs to systems identification, process control, prediction, diagnosis, etc. In the area of power electronics, the application of NN has achieved great improvements, and the future looks promising [12].

The goal is to obtain a simple implementation, in real time, of the control strategy described before. In this way, the utilization of NN on systems identification, and particularly, the approximation of the optimization function previously elaborated appear like an interesting solution [13]. Consequently, as a first step the optimization system was numerically resolved for 30 city-drive data sets, obtaining the required input and output data.

The following where used as the net input data: load current $(I_{\rm load})$, load power $(P_{\rm load})$, vehicle speed (v), and the kinetic energy (E) contained on it. All at instants k and $k-1$. The data output from the net is the ideal current that the UCAPs $(I_{\rm uc})$ must deliver. The Levenberg–Marquardt algorithm was used to train the net, which is characterized by its fast convergence and robustness. Then, to define the ideal net architecture, "prunning" algorithms where used, in particular the "optimal brain surgeon" (OBS) algorithm [14], [15] was applied. Finally, to validate the net, the mean quadratic error was analyzed. From a universe of 30 data sets, 10 of them were used as training data, and 20 as validation data. Fig. 8 shows the net's architecture, obtained from OBS algorithm. Fig. 9 shows the results for one of the validation data set.

TABLE II
ROAD TESTS RESULTS (COMPARISON OF DIFFERENT CONTROL STRATEGIES)

	Km/KWh	Km/KWh Improvement
Batteries with AES (SOC Control)	3.25	-
Batteries with AES (Optimal Neural Network Control)	3.36	3.3%

As shown in Fig. 8, the optimal current approximation delivered by the NN is used as reference for a PI-current control, at the low-voltage side of the buck–boost converter.

Finally, the NN's useful implementation has been done in a serial way, using a high-speed DSP (TMS320F241). The

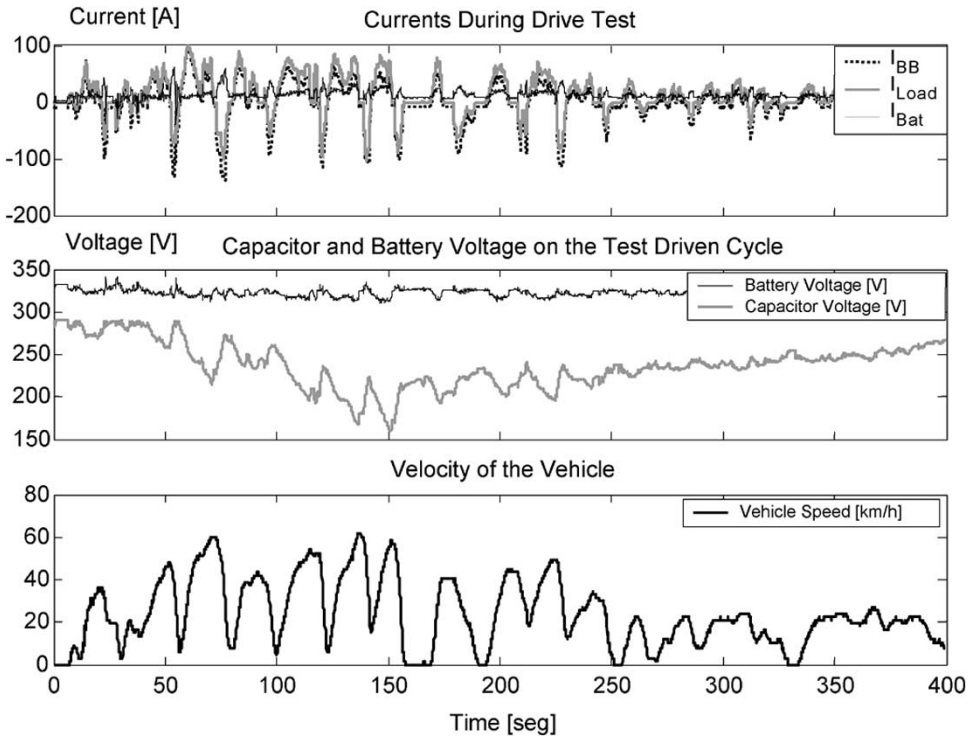

Fig. 10. Fragment of drive-test currents, voltages, and vehicle speed.

buck–boost control works at 12 kHz; nevertheless, as the system is characterized for its slow dynamics, the reference is updated only at 11 Hz.

VIII. Practical Results

An urban test course of 14.2 km has been designed. Four different tests where performed: 1) batteries only, without regeneration (to emulate the behavior of a vehicle running on fuel cells or zinc-air batteries only); 2) batteries only, but with regeneration capability; 3) batteries and AES (UCAPs) with SOC control; and 4) batteries and the AES, using optimal control implemented with NNs. Mean values of tests results where calculated after numerous tests performed, which are shown in Tables I and II.

According to Table II, with optimal-control strategy proposed, the km/kWh indicator is improved in 3.3% respect to the UCAPs SOC control strategy.

Fig. 10 shows a fragment of currents, voltages, and speed signals from the vehicle during tests.

Another important characteristic of the system is that maximum power delivered by the primary source was dramatically reduced, from 54 to 12 kW.

IX. Conclusion

A new control strategy for an HEV vehicle was presented in this paper. This strategy was elaborated based on efficiency characteristics of the AES conformed by UCAPs and a buck–boost converter. In order to do this, an optimal-control model has been formulated, the numerical solution has been reached and the model simulated. Thereafter, a theoretical efficiency improvement of 4.9% from the original strategy based on UCAPs SOC was calculated. To test this new strategy on the field, an NN was trained based on results obtained from simulations of different driving cycles. A DSP (TMS320F241) has been used for its real-time implementation.

After numerous city driving tests, a 3.3% improvement compared to SOC control strategy was obtained in terms of km/kWh. On the other hand, if a primary source unable to receive regeneration energy is considered, then the improvement would be of 28.7% in terms of km/kWh.

References

[1] O. Fuji, "The development and application of hybrid vehicles," in *Proc. 19th Int. Electr. Vehicle Symp.*, Busan, Korea, Oct. 19–23, 2002, CD-ROM.

[2] F. A. Wyczalek, "Hybrid electric vehicles, year 2000 status," *IEEE Aerosp. Electron. Syst. Mag.*, vol. 16, no. 3, pp. 15–25, Mar. 2001.

[3] A. F. Burke and M. Miller, "Comparisons of ultracapacitors and advanced batteries for pulse power in vehicle applications: Performance, life, and cost," in *Proc. 19th Int. Electr. Vehicle Symp.*, Busan, Korea, Oct. 19–23, 2002, CD-ROM.

[4] A. F. Burke, "Ultracapacitors: Why, how, and where is the technology," *J. Power Sources*, vol. 91, no. 1, pp. 37–50, Nov. 2000.

[5] B. J. Arnet and L. P. Haines, "Combining ultra-capacitors with lead-acid batteries," in *Proc. 17th Int. Electr. Vehicle Symp.*, Montreal, QC, Canada, Oct. 13–18, 2000, CD-ROM.

[6] J. Dixon, M. Ortúzar, and E. Wiechmann, "Regenerative braking for an electric vehicle using ultracapacitors and a buck-boost converter," in *Proc. 17th Int. Electr. Vehicle Symp.*, Montreal, QC, Canada, Oct. 13–18, 2000, CD-ROM.

[7] *Power Electronics Handbook*, Academic, San Diego, CA, 2001.

[8] G. Paganelli, T. M. Guerra, S. Delprat, Y. Guezennrc, and G. Rizzoni, "Optimal control theory applied to hybrid fuel cell powered vehicle," in *Proc. 15th IFAC World Congr. Automatic Control*, Barcelona, Spain, 2002, CD-ROM.

[9] S. Delprat, T. M. Guerra, and J. Rimaux, "Optimal control of a parallel powertrain: From global optimization to real time control strategy," in *Proc. 18th Int. Electr. Vehicle Symp.*, Berlin, Germany, Oct. 2001, CD-ROM.

[10] Y. Guezennrc, T. Choi, and G. Paganelli, "Supervisory control of fuel cell vehicles and its link to overall system efficiency and low-level control requirements," in *Proc. IGERT Graduate Student Res. Conf.*, Davis, CA, Jun. 2003, pp. 2055–2061.
[11] R. Stegel, *Optimal Control and Estimation*. New York: Dover, 1994, pp. 201–259.
[12] B. K. Bose, "Artificial neural network applications in power electronics," in *Proc. IEEE IECON*, Nov. 29–Dec. 2, 2001, pp. 1631–1638.
[13] S. Haykin, *Neural Networks: A Comprehensive Foundation*. Englewood Cliffs, NJ: Prentice-Hall, 1998, pp. 208–213.
[14] M. Nørgaard, N. K. Poulsen, O. Ravn, and L. Hansen, *Neural Networks for Modelling and Control Dynamic System*. New York: Springer-Verlag, 2000, ch. 2.
[15] M. Nørgaard, "Neural network based system identification toolbox," Dept. Automation, Tech. Univ. Denmark, Lyngby, Denmark, Tech. Rep. 00-E-891, 2000.

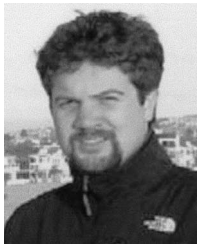

Jorge Moreno (S'04–M'06) received the B.S. and M.Sc. degrees in electrical engineering from Pontificia Universidad Católica de Chile, Santiago, Chile, in 2004.

He served an internship in the Sciences des Processus Industriels et Naturels (SPIN) Department at l'Ecole Nationale Supérieure des Mines de Saint Etienne, France. He has worked in automatic control, power electronics, and electric vehicles (EVs) research projects. He is currently a Consultant Engineer with Systep Engineering and Design Company.

Micah E. Ortúzar (S'02–M'04) was born in Santiago, Chile. He received the Electrical Engineering Professional degree in 2001 from Pontificia Universidad Católica de Chile, Santiago, Chile, where he is currently working toward the Ph.D. degree.

Since 2000, he has been working in power electronics and electric vehicle research projects, involving active power filters, static converters, ultracapacitors, and electric machines among others. He has written and published several papers for IEEE conferences, as principal author and coauthor, and is a coauthor in three papers published in IEEE magazines and transactions.

Juan W. Dixon (M'90–SM'95) was born in Santiago, Chile. He received the Electrical Engineering Professional degree from the University of Chile, Santiago, Chile, in 1977, and the M.-Eng. and Ph.D. degrees in electrical engineering from McGill University, Montreal, PQ, Canada, in 1986 and 1988, respectively.

Since 1979, he has been with Pontificia Universidad Católica de Chile, Santiago, Chile, working in the areas of power electronics, electric traction, electric power generation, and electrical machines. He is currently a Professor at the Department of Electrical Engineering. His research interests include new technologies for electric vehicles, machine drives, frequency changers, high-power rectifiers, multilevel inverters, static VAr compensators, and active power filters.